OPTOELECTRONICS AND ADVANCED MATERIALS – RAPID COMMUNICATIONS Vol. 7, No. 11-12, November - December 2013, p. 881-886

Chemical composition and processing effects on the pseudoelastic response of α' ferromagnetic martensite

A. L. PARASCHIV[a], F. BORZA[b], M.-G. SURU[a], B. PRICOP[b], I. P. SPIRIDON[a], E. MIHALACHE[a], L.-G. BUJOREANU[a]*

[a] *Faculty of Materials Science and Engineering, The "Gheorghe Asachi" Technical University of Iaşi, Bd. D. Mangeron 67, 700050 Iaşi, Romania*

[b] *National Institute of Research and Development for Technical Physics, D. Mangeron 47, 700050 Iaşi, Romania*

Processing effects caused by homogenization heat treatment, hot rolling and solution treatment in three Fe-Cr-Ni-C alloys, with different Ni amounts, were analysed by optical and scanning electron microscopy. X-Ray diffraction (XRD), magnetic hysteresis data, Vickers micro-hardness and micro-indentation measurements were used in order to reveal chemical composition and processing effects. Dendrite fragmentation, caused by hot rolling and thermoelastic softening induced by solution treatment, in parallel with the substitution of a part of Cr with Ni, were reported and discussed. Structural changes were corroborated with the variations of magnetic (hysteresis) and mechanical (micro-hardness and micro-indentation) properties. The pseudoelastic character of Fe-Cr-Ni-C alloys was revealed in association with anelastic effect, determined by the variation rate in time of the average dimension of Vickers micro-hardness-induced notch. The confirmation of the pseudoelastic character of the alloys under study was found in the load-depth variations recorded within micro-indentation tests.

(Received July 1, 2013; accepted November 7, 2013)

Keywords: Fe-Cr-Ni-C alloy, Microscopy, Microstructure, Magnetism, Pseudoelasticity

1. Introduction

There are presently five commercial Shape Memory Alloy (SMA) systems based on Ni-Ti, Cu-Zn-Al, Cu-Al-Ni, Fe-Mn and Fe-Ni [1]. Fe-Ni alloys system experiences a reversible martensitic transformation of the type γ (face centre cubic, fcc) ↔ α' (body centre cubic, bcc), characterized by a thermal hysteresis of approx. 400 K [2]. Various attempts were made to reduce thermal hysteresis, by ternary alloying with:

(i) C, which led to Fe-(27-31) Ni-(0.4-0.8) C, mass % as all chemical compositions will be given hereinafter, SMAs [3] with martensite tetragonality degree increasing while passing from lenticular to plate-like morphologies [4];

(ii) Mn, which has enabled the obtainment of Fe-(22-26) Ni-(2-4) Mn SMAs [5] with isothermal martensite transformation [6];

(iii) Nb, enabling the occurrence of perfect Shape Memory Effect (SME) in ausaged Fe-(30.9-31) Ni-(4.6-6.8) Nb SMAs [7];

(iv) Co, based on which Fe-(25-33) Ni-(10-20) Co-(3-4) Ti SMAs were developed [8] which further evolved to Fe-Ni-Co-Al-Ta-B alloys with superelastic strains above 13 % [9];

(v) Cr, usually present in austenitic stainless steels, with typical compositions including about 16-26 Cr, 7-30 Ni and up to 0.15 C [10].

Fig. 1 illustrates a room temperature, (RT) isothermal section, of ternary Fe-Cr-Ni phase diagram (for 0.04 C). In Fe-Ni-Cr base alloys the presence of α' ferromagnetic martensite [11] was reported as beneficial for the occurrence of pseudoelasticity [12].

This paper aims to emphasize the effects of both Chromium substitution with Nickel and thermomechanical processing on magnetic and pseudoelastic properties of α' martensite.

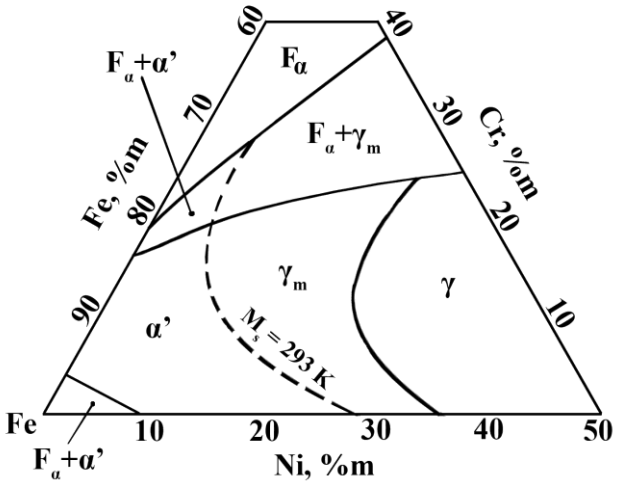

Fig. 1. RT partial isothermal section through metastable Fe-Ni-Cr phase diagram (0.04 % C) illustrating the locus of the alloys with M_s = 293 K [11].

2. Experimental procedure

Three alloys, with nominal chemical compositions Fe-10Cr-3Ni, Fe-9Cr-4Ni and Fe-7Cr-5Ni, were prepared by induction melting under Ar atmosphere, cast into cylindrical moulds and homogenized for 8 × 3.6 ks at 1300 K. After cutting some fragments for structural analysis, the homogenized rods were hot rolled at 1273 K. After 8 rolling passes, the thickness decreased to 0.9×10^{-3}m. Some fragments were cut, from hot rolled specimens, for structural analysis and the rest of the specimens were solution treated 1300 K/ 1.8 ks/ water. The fragments cut from homogenized (HOM), hot rolled (HR) and solution treated (ST) samples, respectively, were embedded into could mounting resign, ground and polished and finally etched with Nital 4 %.

Optical microscopy (OM) micrographs were recorded with a Meiji TECHNO microscope equipped with a video camera and QCapture software while scanning electron microscopy (SEM) micrographs were obtained by means of a SEM—VEGA II LSH TESCAN microscope, coupled with an EDX—QUANTAX QX2 ROENTEC detector, which gave chemical compositions listed in Table 1.

Table 1. Chemical compositions determined by EDX, mass. %.

Element	Nominal alloy		
	Fe-10Cr-3Ni	Fe-9Cr-4Ni	Fe-7Cr-5Ni
Iron	86.22	85.95	87.63
Chromium	10.25	9.5	7.19
Nickel	3.06	4.22	4.88
Carbon	0.47	0.33	0.3

X-Ray diffraction measurements were performed on ST specimens using a D8 Advance - Bruker AxS GmbH diffractometer with Cu-K_α radiation, radiation intensity I_e=40mA and Voltage= 40KV.

Magnetic measurements were performed with Lakeshore vibrating sample magnetometer (VSM) at maximum field of 10 kOe.

Vickers micro-hardness ($HV_{0.2}$) tests were done with a CV 400 DM Namicon tester under a load of 0.2 kg applied for 25 s. Impression mark measurements were repeated 5 times, every minute, aiming to reveal anelastic effects [13].

Micro-indentation tests were performed with a UMT-CETR universal tester [14] at a maximum load of 13.5 N. Load-depth indentation curves were recorded, at a position precision of 1×10^{-7}m, by means of the CETR data viewing software, able to determine hardness and Young modulus values.

2. Results and discussion

OM micrographs with SEM insets of HOM specimens are shown in Fig. 2. In spite of 8 × 3.6 ks holding at 1300 K, Cr-rich dendrites are still present. Dendrite dissolution seems to be enhanced by Cr substitution with Ni being accompanied by the occurrence of small precipitate islands, better revealed in SEM inset of Fig. 2(c).

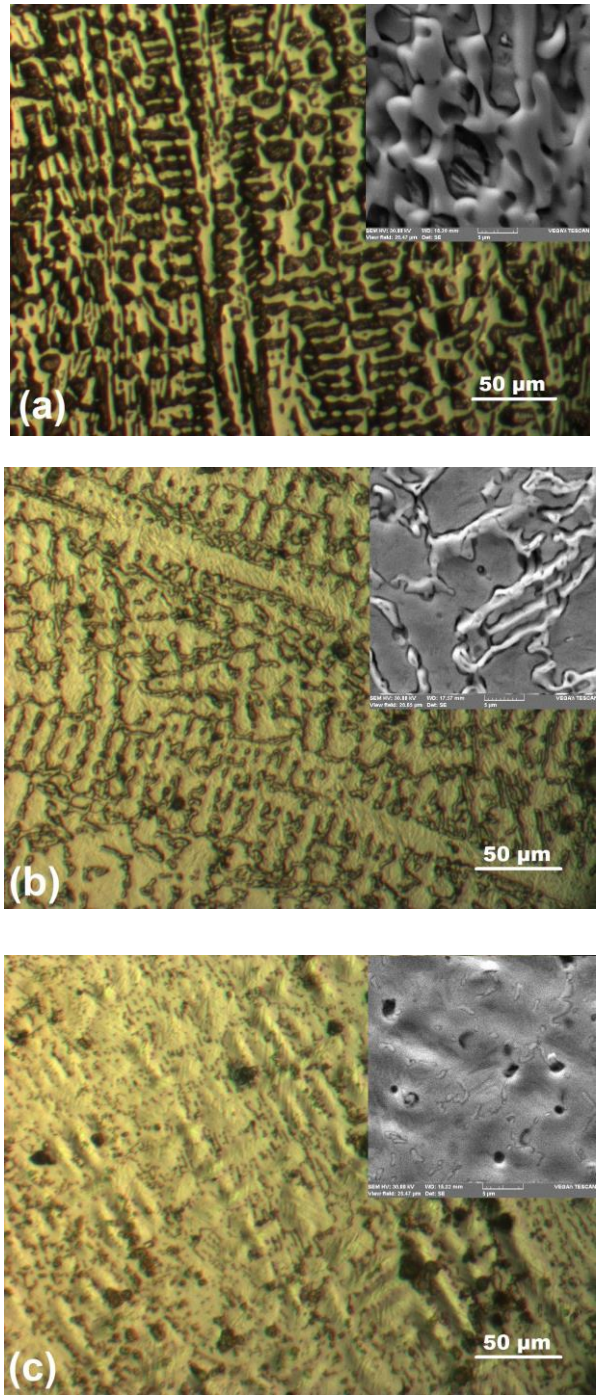

Fig. 2. OM micrographs with 10 time magnified details in SEM insets of HOM specimens: (a) Fe-10Cr-3Ni; (b) Fe-9Cr-4Ni; (c) Fe-7Cr-5Ni.

Fig. 3 shows that, after 8 hot-rolling passes, most of the dendritic arms were broken. Due to the higher Carbon content, (0.3-0.47 C), the structure of HR specimens differs from Fig. 1, corresponding to 0.04 C. The expected phases are Chromium-rich alpha ferrite, F_α and alloy pearlite, consisting in a eutectoid mixture of F_α and $M_{23}C_6$-type carbide which in this case is $Cr_{23}C_6$ [15].

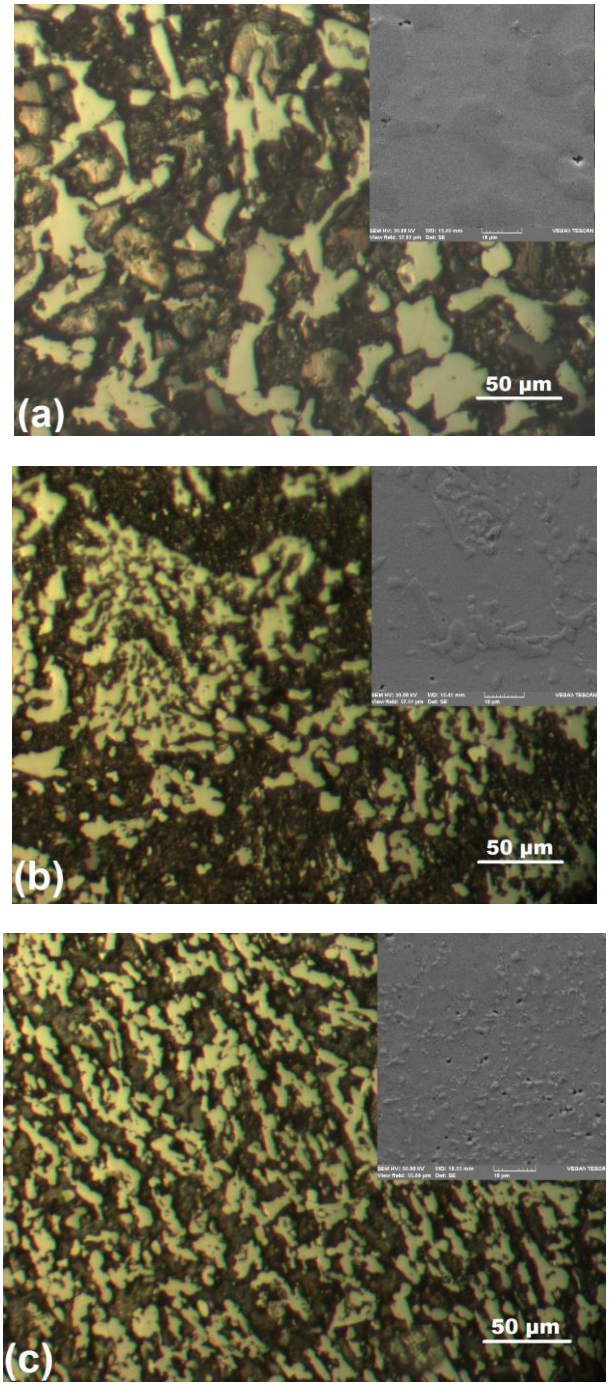

Fig. 3. Typical OM micrographs with 5 time magnified details in SEM insets of HR specimens: (a) Fe-10Cr-3Ni; (b) Fe-9Cr-4Ni; (c) Fe-7Cr-5Ni.

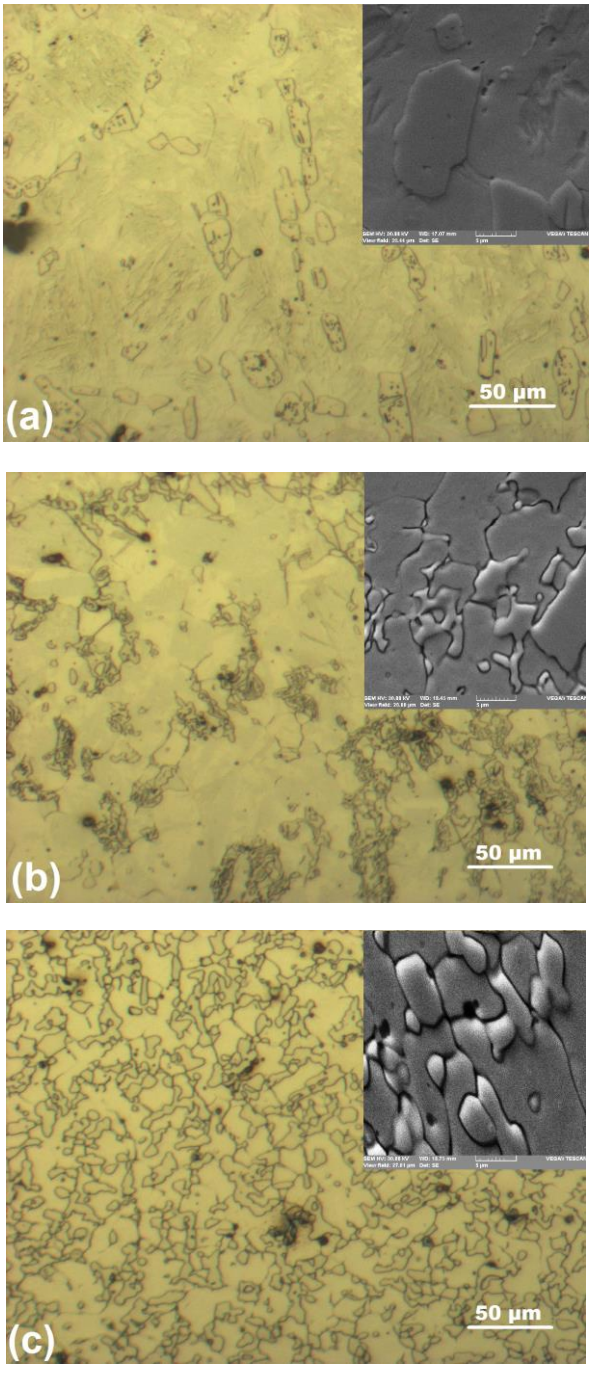

Fig. 4. Typical OM micrographs with 10 time magnified details in SEM insets of precipitate structures caused by solution treatment in specimens: (a) Fe-10Cr-3Ni; (b) Fe-9Cr-4Ni; (c) Fe-7Cr-5Ni.

The effects of solution treatment, for half hour at 1300 K followed by water quenching, are illustrated in Fig. 4.

Assuming the occurrence of full austenitization throughout high temperature maintaining [16], water quenching is expected to cause thermally induced formation of α' martensite [17]. Fig. 4 suggests that the three ST alloys under study have tri-phase structure, possibly α' martensite (bcc), γ retained austenite (fcc) and scarce carbide precipitates.

In order to ascertain this structure, XRD patterns were recorded as shown in Fig. 5. As noticeable, on each XRD pattern of solution treated (ST) specimens, in Fig. 5(a), the main diffraction maximum can be ascribed to martensite as α'(110). The other maxima belonging to martensite are α'(200) and α'(211). In addition, there are three diffraction maxima which can be ascribed to retained austenite, as γ(111), γ(200) and γ(220) [18].

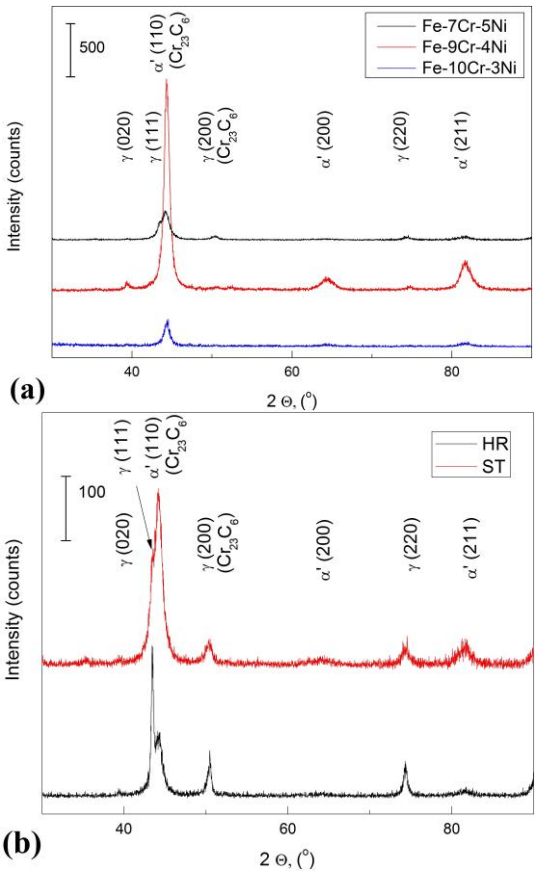

Fig. 5. XRD patterns of the alloys under study: (a) in solution treated (ST) state; (b) comparison between solution treated (ST) and hot rolled (HR) states in specimen Fe-7Cr-5Ni.

The peaks of both α'(110) and γ(200) overlap on two of the XRD maxima of $Cr_{23}C_6$ so carbide presence can also be considered, when evaluating the structure of ST specimens. On the other hand, it is noticeable that the main peak of retained austenite, γ(111), partially overlaps on α'(110), the main peak of martensite. However, it is only in the specimen Fe-7Cr-5Ni, with has the largest Ni content, where γ(111) is distinctively noticeable. Thus, the solution treated structure assumed from OM micrographs, comprising α' martensite, γ retained austenite and carbide precipitates, was confirmed by XRD patterns, the amount of γ increasing with Ni content. On the other hand, a comparison of XRD patterns of specimens Fe-7Cr-5Ni, in solution treated (ST) and hot rolled (HR) states, shows in the latter the presence of two prominent maxima at $2\Theta = 44.2^0$ and 50.5^0, respectively, figure 5(b). These peaks, characteristic to HR state, could correspond to α'(110) and γ(200), respectively but they can also be ascribed to the main (100 %) and the third (60 %) diffraction maxima of Chromium carbide $Cr_{23}C_6$ [11]. In order to confirm the presence of γ austenite in HR or in ST state, magnetic measurements were performed.

The variations of magnetic properties, determined by VSM, are revealed by the shape of magnetic hysteresis loops illustrated in Fig. 6. As noticeable, with increasing nominal Nickel amount, from 3 to 4 and further to 5 %, the value of saturation magnetization decreases, which suggests the increase of the proportion of paramagnetic γ-phase, in good agreement with XRD patterns.

For the alloys with 3 % Ni, Fig. 6(a) shows that solution treated (ST) state is characterized by higher values of saturation magnetization as compared to hot rolled (HR) state. This effect can be ascribed to the thermally induced martensitic transformation of austenite, during water quenching, within solution treatment. Since paramagnetic γ-phase transformed to ferromagnetic α' martensite, magnetization became larger in ST than in HR state, at specimen Fe-10Cr-3Ni. A summary of magnetic parameters is given in Table 2.

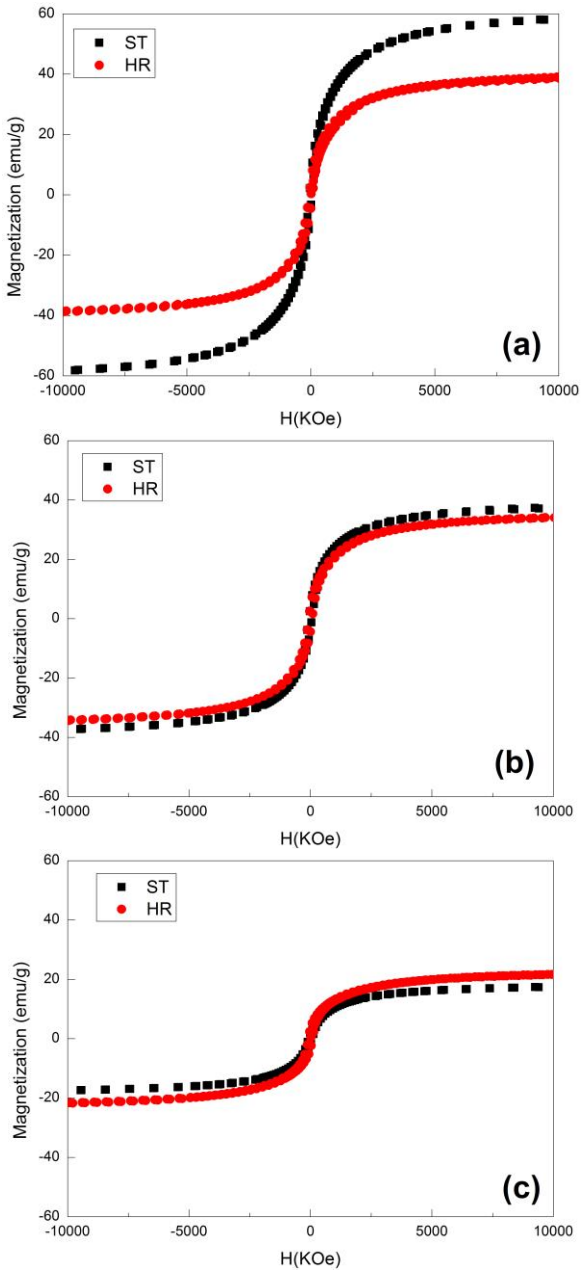

Fig. 6. Variation of magnetization with magnetic field intensity (H), for hot rolled (HT) and solution treated states (ST) of the in specimens: (a) Fe - 10Cr - 3Ni; (b) Fe-9Cr-4Ni; (c) Fe-7Cr-5Ni.

Table 2. Experimental parameters determined from magnetic measurements illustrated in Fig. 6.

Alloy	Fe-10Cr-3Ni		Fe-9Cr-4Ni		Fe-7Cr-5Ni	
State	HR	ST	HR	ST	HR	ST
Coercivity (Oe)	68.5	53.6	74.1	61.2	84.9	79.2
Magnetization (emu/g)	40.0	60.0	35.4	38.7	22.7	18.3
Squareness (10^{-3})	109.8	80.5	120.8	94.1	146.2	126.3

Figs. 6(b) and (c) show that, for the alloys with 4 and 5 % Ni, the difference between the magnetizations of HR and ST states is very slight. This could be ascribed to the presence of carbides in HR specimens, causing the deterioration of the soft magnetic properties [11].

Assuming the presence of α' martensite in ST specimens, Vickers micro-hardness ($HV_{0.2}$) measurements were performed. After removing the load, impression mark measurements were repeated every minute, for 5 times. The results are summarized in Table 3 and Fig. 7.

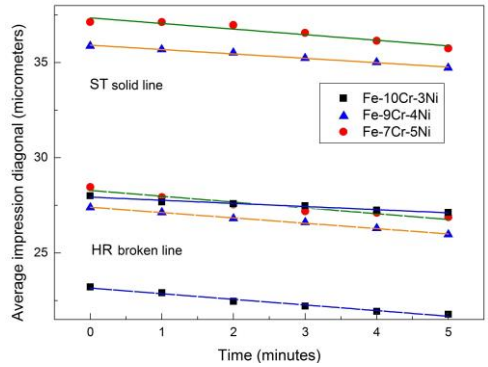

Fig. 7. Illustration of pseudoelastic character by the variation in time of the average diagonal of $HV_{0.2}$ measurements.

Table 3. Vickers hardness values ($HV_{0.2}$) and variation rate of average impression diagonal determined from linear fit in Fig. 7.

Alloy	Parameter	HR	ST
Fe-10Cr-3Ni	$HV_{0.2}$ (daN/ mm^2)	688	473
	∂d/ ∂t (μm/min)	0.296	0.165
Fe-9Cr-4Ni	$HV_{0.2}$ (daN/ mm^2)	458	269
	∂d/ ∂t (μm/min)	0.305	0.294
Fe-7Cr-5Ni	$HV_{0.2}$ (daN/ mm^2)	494	288
	∂d/ ∂t (μm/min)	0.280	0.230

First of all, since the increase of impression dimensions can be associated with the decrease of hardness, it is obvious that $HV_{0.2}$ values are lower in ST state than in HR state, due to softening effect caused by the formation of α' thermoelastic martensite [9]. Considering the effects of Cr substitution with Ni, in HR and ST states, respectively, it is known that the increase of Ni amount was accompanied by a general hardening-decrease tendency [8].

The pseudoelastic character of the alloys under study caused a sensible reduction in time of the size of indentation marks impressed on the surface of specimens, as illustrated in Fig. 7. Linear fits of impression variation with time were performed by ORIGIN software and the slopes, ∂d/ ∂t listed in Table 3, represent the variation rate tendencies of average impression dimension.

The impression values of ST alloys are larger than those of HR alloys ascertaining that the former are softer than the latter. For every Ni content, ∂d/ ∂t values have been larger in HT state than in ST state, which proves that α' thermoelastic martensite experiences a lower variation rate of superficial deformation recovery, which slightly tends to augment with the increase of Ni content.

Since both pseudoelasticity and anelastic effect are associated with the reversible motion of twin boundaries [19] it can be stated that lower variation rates of superficial deformation recovery can be indicative of a more enhanced pseudoelastic character of the alloys under study.

The pseudoelastic response of the alloys in ST state has been ascertained by the micro-indentation curves displayed in Fig. 8.

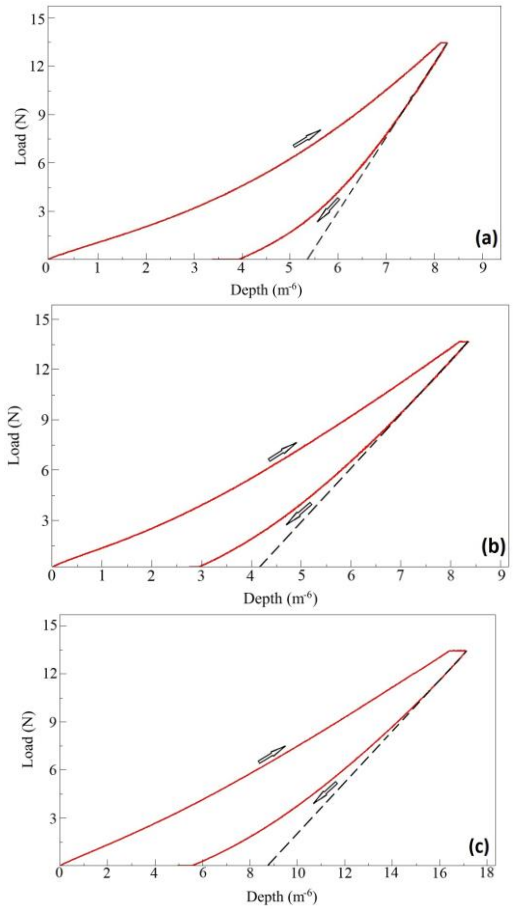

Fig. 8. Micro-indentation curves, at a maximum load of 13.5 N, illustrating the increase of pseudoelastic character with Ni amount in solution treated states (ST) of the in specimens: (a) Fe-10Cr-3Ni; (b) Fe-9Cr-4Ni; (c) Fe-7Cr-5Ni.

As known, pseudoelasticity refers to any non-linearity occurring on the unloading portion of a stress-strain curve [13]. In Fig. 8 the magnitude of the pseudoelastic spring back can be evaluated by the difference between the intersections with abscissa of linear unloading (dashed line) and actual unloading (descending arrow) [20]. The representative mechanical parameters are summarized in Table 4.

Table 4. Mechanical characteristics determined from micro-indentation curves of ST specimens, in Fig. 8.

	Hard-ness	Young modulus	Maxi-mum displa-cement	Pseudo-elastic spring-back	Pseudo-elastic response %
	GPa	GPa	10^{-6} m	10^{-6} m	%
Fe-10Cr-3Ni	2.085	46.1	1.3	8.2	16
Fe-9Cr-4Ni	1.422	15.457	1.2	8.3	15
Fe-7Cr-5Ni	0.949	10.736	3.1	17.1	18

Here, again, the partial substitution of Cr with Ni caused the increase of austenite amount, accompanied by a softening tendency, reflected by the variations of hardness and Young modulus. On the other hand, the increase of Ni amount from 3 to 5, has been accompanied by a general increasing tendency of both pseudoelastic spring back, from 8.2 to 17.1×10^{-6}m and pseudoelastic response, from 16 to 18 %.

4. Conclusions

The evolution of structure and properties was studied in three Fe-Cr-Ni alloys, with 0.3-0.47 mass. % C, during thermomechanical processing and partial substitution of Chromium with Nickel within the limits 10 Cr-3Ni and 7 Cr-5Ni (m%).

Hot rolled structure, considered as a mixture of alloy alpha ferrite and Chromium carbides, was characterized by low values of saturation magnetization, between 40 and 22 emu/ g, and high Vickers micro-hardness, between 688 and 494 daN/mm^2. Both magnetization and hardness values tend to decrease with increasing Ni content.

Solution treated structure, considered as α' thermoelastic martensite, γ retained austenite and scarce precipitated $Cr_{23}C_6$ carbides, showed magnetizations ranging between 60 and 18 emu/ g, and micro-hardness values, between 473 and 288 daN/mm^2. In solution treated state, as well, both magnetization and hardness tend to decrease with increasing Ni content.

In solution treated state, the pseudoelastic response was associated with the presence of α' thermoelastic martensite, stabilized by reciprocal blocking of differentially oriented martensite populations [21]. Pseudoelastic increased nickel content, from 16 %, at 3 Ni to 18 % at 5 Ni.

Acknowledgements

This paper was financially supported by the project PN.II-PT-PCCA-2011-3.1-0174, contract no. 144.

References

[1] L. Sun, W. M. Huang, Z. Ding, Y. Zhao, C. C. Wang, H. Purnawali, C. Tang, Mater. Design **33**, 577 (2012).
[2] L. Kaufman, M. Cohen, Progress in Metal Physics **7**, 165 (1958).
[3] S. Kajiwara, T. Kikuchi, Acta Metall. Mater. **38**(5), 847 (1990).
[4] S. Kajiwara, T. Kikuchi, Acta Metall. Mater. **39**(6), 1123 (1991).
[5] S. Kajiwara, Philos. Mag. **43**(6), 1483 (1981).
[6] S. Kajiwara, Acta Metall. **32**(3), 407 (1984).
[7] Yu. N. Koval, G. E. Monastirsky, Scripta Metall. Mater. **28**, 41 (1993).
[8] N. Jost, Progress in Shape Memory Alloys, Ed. S. Eucken, Informationgesellschaft Verlag, Bochum, 1992, p. 173.
[9] Y. Tanaka, Y. Himuro, R. Kainuma, Y. Sutou, T. Omori, K. Ishida, Science **327**, 1488 (2010).
[10] A. K. Sinha, Ferrous Physical Metallurgy, Butterworth, 1989, p. 327-369.
[11] S. Yokoyama, T. Inui, Y. Minamino, J. Mater. Sci. **38**, 4535 (2003).
[12] G. B. Brook, R. F. Iles, P. L. Brooks, Shape Memory Effects in Alloys, Ed. J. Perkins, Plenum Press, New York, 1975, p. 477.
[13] T. W. Duerig, R., Zadno, Engineering Aspects of Shape Memory Alloys, Eds. T. W. Duerig, K. N. Melton, D. Stöckel, C. M. Wayman, Butterworth-Heinemann, 1990, p 369.
[14] J. Gearing, Mater. World **16**(1), 32 (2001).
[15] H. K. D. H. Bhadeshia, Sir R. Honeycomb, Steels. Microstructure and Properties. Third Edition, Elsevier, 2006, p. 80.
[16] J. C. Anderson, K. D. Leaver, R. D. Rawlings, J.M. Alexander, Materials Science. Fourth Edition, Chapmann and Hall, London, 1990, p 269.
[17] T. Angeliu, E. Hall, M. Larsen, A. Linsebigler, C. Mukira, Metall. Mater. Trans. A **34**A, 927 (2003).
[18] T. Volkmann, W. Löser, D.M. Herlach, Metall. Mater. Trans. A **28**A, 461 (1997).
[19] H. Numakura, K. Hasegawa, M. Koiwa, Acta. Mater. **40**(6), 1365 (1992).
[20] S. Stanciu, L. G. Bujoreanu, R. I. Comăneci, N. Cimpoeșu, I. Ioniță, V. V.Moldoveanu, Proc. ESOMAT 2009, 05004 (2009).
[21] L. G. Bujoreanu, N.M. Lohan, B. Pricop, N. Cimpoeșu, J. Mater. Eng. Peform. **20**, 468 (2011).

*Corresponding author: lgbujor@yahoo.com